nature chemical engineering

Article

https://doi.org/10.1038/s44286-023-00001-5

Flexible hemline-shaped microfibers for liquid transport

Received: 11 April 2023

Accepted: 20 November 2023

Published online: 11 January 2024

Check for updates

Chaoyu Yang [1,2,4], Yunru Yu [1,2,4], Luoran Shang [3] ✉ & Yuanjin Zhao [1,2] ✉

Directional liquid transport is important in both fundamental studies and industrial applications. Most existing strategies rely on the use of predesigned surfaces with sophisticated microstructures that limit the versatility and universality of the liquid transport. Here we present a platform for liquid transport based on flexible microfluidic-derived fibers with hemline-shaped cross-sections. These microfibers have periodic parallel microcavities along the axial direction, with sharp edges and wedge corners that enable unilateral pinning and capillary rise of liquids. This structure enables directional liquid transport along hydrophilic substrates with the use of a single fiber. Alternatively, a pair of fibers enables directional liquid transport along hydrophobic substrates or even without any additional substrate; the directional transport behavior applies to a wide range of liquids. We demonstrate the use of these fibers in open microfluidics, water extraction and liquid transport along arbitrary three-dimensional paths. Our platform provides a facile and universal solution for directional liquid transport in a range of different scenarios.

Directional liquid transport is important in both fundamental research and practical applications including oil–water separation[1–3], liquid pumping[4,5], water harvesting[6,7] and microfluidics[8–13]. Numerous efforts have been made to design microscale systems that exploit driving forces, including the use of surface tension gradients[14,15], external impetus[16–19], chemical gradients[20–22] and biomimetic anisotropic structures[23–32]. In addition, to ensure survival, some natural organisms have evolved surface structures to generate unbalanced forces and control directional liquid dynamics[1,7,22,33]. Inspired in part by this, fibrous materials with flexible shapes and asymmetric microstructures obtained through electrospinning, three-dimensional (3D) printing and microfluidics have garnered substantial attention for liquid transport[34,35]. For example, microfibers inspired by spider silk and with a spindle-knotted structure have been designed with anisotropic curvature and surface roughness that induce liquid transport by combining the surface tension gradient arising from variations in surface roughness and the Laplace pressure difference caused by the curvature gradient[36]. Therefore, precise control over the direction, speed and distance of liquid transport on substrates with a predesigned surface architecture has been widely achieved[5,33,37–42]. Despite this progress, transport of different types of liquid remains challenging because the surface energies of the liquid and surface(s) impacts the resulting transport behavior. Furthermore, the manipulation of liquids in desired 3D paths is even more difficult due primarily to challenging microfabrication[24,43,44]. Therefore, platforms with directional transport capabilities for a range of liquids and transport pathways are required to bridge the gap between studies of fundamental liquid dynamics and practical applications.

In this study, we fabricate flexible hemline-shaped fibers from microfluidics (Fig. 1a) as an alternative to the widely adopted strategy of using a predesigned surface with sophisticated microstructures. So far, microfluidics has been extensively employed to create microfibers with cross-sectional shape anisotropy by geometric confinement[45,46] or inertial flow[34,47,48]. However, few studies have explored

[1]Department of Rheumatology and Immunology, Nanjing Drum Tower Hospital, School of Biological Science and Medical Engineering, Southeast University, Nanjing, China. [2]Oujiang Laboratory (Zhejiang Lab for Regenerative Medicine, Vision and Brain Health), Wenzhou Institute, University of Chinese Academy of Sciences, Wenzhou, China. [3]Zhongshan-Xuhui Hospital, and the Shanghai Key Laboratory of Medical Epigenetics, the International Co-laboratory of Medical Epigenetics and Metabolism, Ministry of Science and Technology (Institutes of Biomedical Sciences), Fudan University, Shanghai, China. [4]These authors contributed equally: Chaoyu Yang, Yunru Yu. ✉e-mail: luoranshang@fudan.edu.cn; yjzhao@seu.edu.cn

https://doi.org/10.1038/s44286-023-00001-5

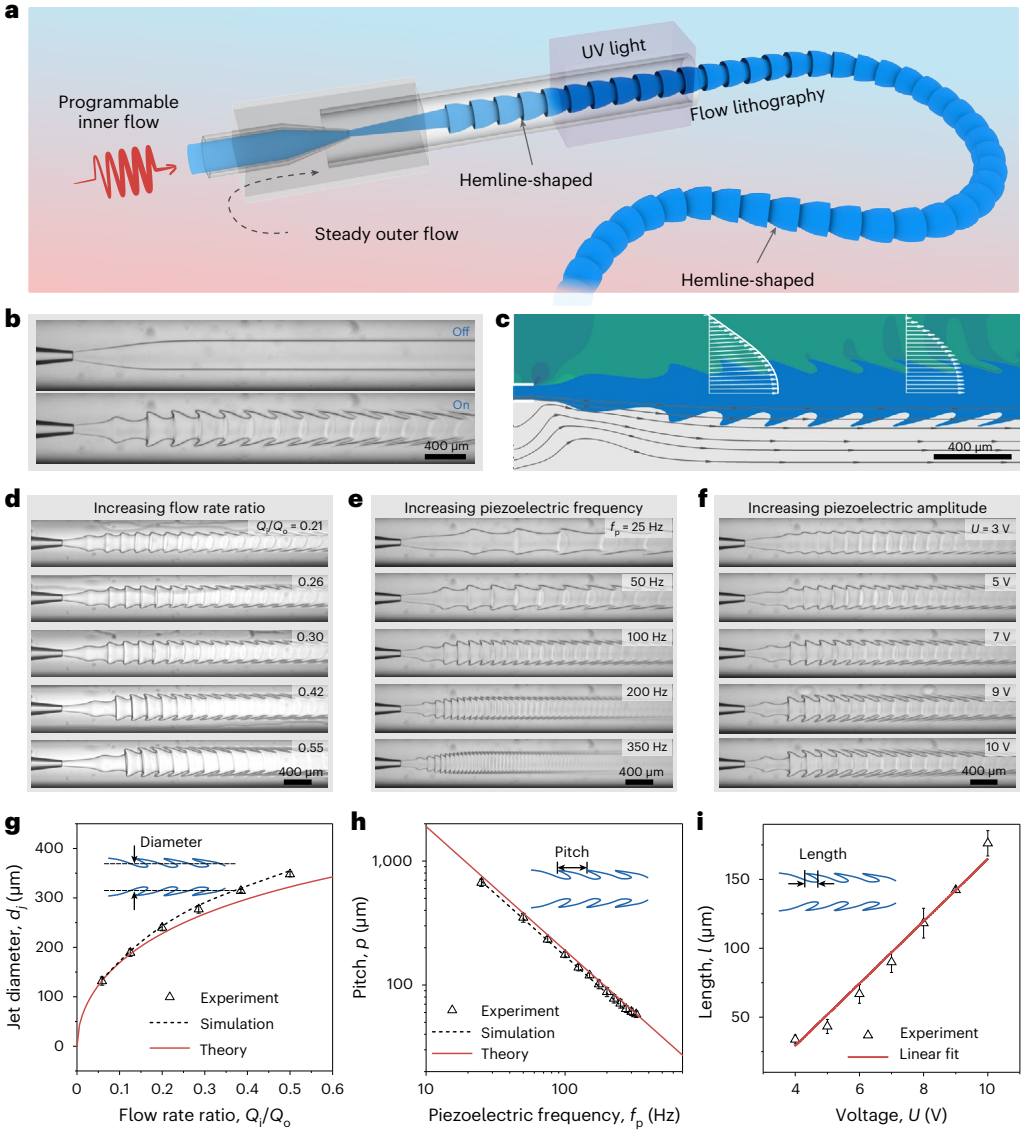

Fig. 1 | Generation of a hemline-shaped jet template from piezoelectric microfluidics. a, Schematic of the spinning process of the hemline-shaped microfiber with programmable hemlines by piezoelectric-induced fluid vibration in a microfluidic channel. **b**, High-speed snapshots of a stable jet and a hemline-shaped jet (Q_i = 4 ml h^{-1}, Q_o = 14 ml h^{-1}, f_p = 80 Hz, U = 7 V). **c**, Computational fluid dynamics simulations of the cross-section flow radial velocity contour and axial velocity profiles (top) and streamline diagram (bottom) during hemline-shaped jet formation corresponding to **b**. **d**–**f**, Real-time images of the hemline-shaped jet under different Q_i/Q_o ($Q_i + Q_o$ = 18 ml h^{-1}, f_p = 80 Hz, U = 6 V; **d**), piezoelectric actuation frequencies (Q_i = 4 ml h^{-1}, Q_o = 14 ml h^{-1}, U = 6 V; **e**) and piezoelectric actuation amplitudes (Q_i = 4 ml h^{-1}, Q_o = 14 ml h^{-1}, f_p = 80 Hz; **f**). **g**, Plot of d_j as a function of Q_i/Q_o. **h**, Plot of p as a function of f_p. **i**, Plot of l as a function of U. Data points and error bars indicate mean values ± s.d. of five measurements in **g**–**i**.

the dynamic control of the axial anisotropy of the resultant fibers. We developed a vibrating flow configuration in a microfluidic channel through piezoelectric control and translated this configuration into solid hemline-shaped microfibers featuring axially aligned cavities with sharp edges and annularly connected wedge corners. When placed on a plain hydrophilic substrate without any specially designed surface architecture, a single microfiber could form an interstice with the substrate and, thus, achieve directional liquid transport. Detailed observation of the transport behavior by high-speed camera revealed that the transport processes included unilateral pinning, continuous transport via the interstice and capillary-rise-induced filling of microcavities. More intriguingly, a pair of close and adjacent fibers with the same or opposite corner orientations were found to give rise to a large variety of liquid transport phenomena that were not restricted to the type of liquid or surface wettability. Most importantly, the microfibers enabled liquid transport along 3D paths because they are intrinsically flexible. On the basis of these advantages, the platform was applied for droplet manipulation, long-distance liquid transport and water–oil separation. These results demonstrate the versatility and universality of the proposed platform; broad applications in open microfluidics, liquid transport along 3D paths, and energy and environmental engineering are envisioned.

Results

Hemline-shaped jet template from piezoelectric microfluidics

The principle behind preparing the hemline-shaped microfibers combines forming a hemline-shaped jet template and solidifying the jet through rapid polymerization. Therefore, a piezoelectric microfluidic system (Supplementary Fig. 1) was constructed to generate a deterministic flow configuration with a coaxially nested capillary chip, in which two fluids flowed concentrically; a piezoelectric actuator is used to program the inner flow dynamically. The inner fluid was a photocurable solution of poly(ethylene glycol) diacrylate (PEGDA), and the outer fluid was pure water. In typical experiments, the range of Reynolds numbers

was approximately 0.8–5.4, indicating flow in the laminar regime. The properties of the inner and outer fluids are listed in Supplementary Table 1. These two fluids are miscible and have negligible interfacial tension, similar to previous studies of aqueous two-phase systems[49,50]. This causes the jet to be easily disturbed and deformed by external fluctuations. A programmed piezoelectric signal was induced to the inner phase, and the interactions between the two-phase interface and external vibrations caused periodic jet oscillations. As a result, the interface was initially folded and then advected by Poiseuille flow in the collection tube, eventually deforming into corrugations with sharp edges (Fig. 1b and Supplementary Video 1).

To investigate the key parameters controlling the polymerized fiber shape and guide experimental design, we performed numerical simulations by solving the mass balance equation and Navier–Stokes equation with the volume-of-fluid model to track the evolution of the fluid/fluid interface. The simulation results revealed that deformation is a result of the expansion and contraction of the jet, with the protruding segment transforming into a hemline shape due to the velocity field gradient within the Poiseuille flow (Fig. 1c, Supplementary Figs. 2 and 19, and Supplementary Video 2). To investigate this further, we conducted a series of experiments by tuning these parameters and measuring the morphology of the jet, as shown in Fig. 1d–f. It was found that the average diameter of the jet, d_j (depicted in Fig. 1g), was positively correlated with the volumetric flow rate ratio of the inner and outer fluids, Q_i/Q_o; these experimental results were consistent with those of the simulations. In this co-flow microfluidic channel, d_j can be derived by applying the conditions of continuity of the velocity field and tangential shear stress as follows[51]:

$$d_j = D_c\left[\frac{(1+\mu\varphi)^{1/2}-(1+\varphi)}{\mu-2-\varphi}\right]^{1/2}, \quad (1)$$

where φ is Q_i/Q_o, μ is the ratio of the inner (η_i) and outer (η_o) viscosities, and D_c is the inner diameter of the collection tube (Supplementary Discussion I). This result is consistent with the experimental measurements (Fig. 1g). In addition, the hemline pitch, p (depicted in Fig. 1h), was negatively correlated with the piezoelectric frequency, f_p. These experimental results were also consistent with the simulation results. Because p also refers to the distance traveled by the jet in an oscillation period ($T = 1/f_p$), it can be represented as $(Q_i \times T)/S$, where S is the jet cross-sectional area and can be calculated as $\pi d_j^2/4$. Taken together, p is given by

$$p = \frac{Q_i}{S}T = \frac{4Q_i(\mu-2-\varphi)}{\pi {D_c}^2 f_p\left[(1+\mu\varphi)^{1/2}-(1+\varphi)\right]}. \quad (2)$$

Theoretical predictions based on equation (2) are in good agreement with those obtained by experiment (Fig. 1h). Moreover, because the voltage, U, affects the amplitude of the vibration, it notably affects the hemline length, l (as depicted in Fig. 1i). These results indicate that the hemline-shaped jet templates can be tailored by adjusting the operational parameters (Supplementary Discussion I).

Microstructure of the hemline-shaped microfibers

To polymerize the jet template, the photoinitiator 2-hydroxy-2-methylpropiophenone (HMPP) was added to the inner fluid. In addition, two ultraviolet (UV) light sources were positioned to irradiate the collection tube in opposite directions, thus concentrating their light to a 0.5 cm × 0.5 cm area (Supplementary Fig. 3). The polymerization timescale must be considerably faster than the time it takes for a jet pass through the irradiation area to ensure that the transient morphology of the liquid jet polymerizes effectively. Moreover, the polymerization timescale is strongly correlated with the UV intensity (I_0), as shown in Supplementary Fig. 4 and Supplementary Discussion II. Therefore, to ensure that the in situ polymerization was sufficiently fast to solidify the transient morphology of the liquid jet, the velocity of the jet, v_j (equation (3)), was controlled with respect to I_0. As a result, hemline-shaped microfibers were generated. Benefiting from the continuous preparation process, meter-scale generation of these hemline-shaped microfibers was achieved with a typical speed of 1.51 cm s^{-1} (Fig. 2a,e). The spinning speed, v_j, was further adjusted by tuning microfluidic parameters (Supplementary Discussion I) according to

$$v_j = \frac{4Q_i(\mu-2-\varphi)}{\pi {D_c}^2\left[(1+\mu\varphi)^{1/2}-(1+\varphi)\right]}. \quad (3)$$

The detailed configuration of the fiber, which consists of periodic parallel microcavities in the axial direction, is shown in Fig. 2b. The pitch and length of the microcavity and diameter of the fiber can be varied by systemically regulating the parameters f_p, U and Q_i/Q_o during jet generation (Supplementary Fig. 5). Furthermore, the resulting hemline-shaped microfibers showed component homogeneity, as confirmed by laser scanning confocal microscopy (Fig. 2d), and unique structural anisotropy, as confirmed by scanning electron microscopy (Fig. 2f). The microcavity was centrosymmetric and annularly connected, with a sharp edge (the radius of curvature, R, was less than 2 µm under a typical set of fiber-generation parameters) and a wedge-shaped corner. To create an adjustable hemline shape, custom-designed fibers with segmented hemlines of varying l, and p along the axis were fabricated by programming different piezoelectric signals (Fig. 3g and Supplementary Fig. 6). These custom-designed fibers could regulate liquid flow dynamically (direction and transport speed). Moreover, the flexibility of the fibers could be controlled by adjusting the PEGDA concentration (Fig. 2c); higher PEGDA concentrations yielded fibers with higher stiffness. Notably, the concentration should not be excessively high because the corresponding high viscosity of the inner phase suppresses jet deformation (Supplementary Fig. 7). To overcome this problem, additional work to enhance the perturbation and deformation of high-viscosity fluids using piezoelectric actuators with larger vibration amplitudes is required.

Liquid transport on flexible surfaces

The sharp edges of the fibers resulted in strong droplet pinning (Supplementary Fig. 8), whereas the wedged corner promoted capillary rise[7,52,53]. When a single hemline-shaped microfiber was placed in contact with a hydrophilic substrate (water contact angle (WCA), $\theta \approx 40°$), water was transported unidirectionally in the forward direction (that is, against the hemline) without retraction, unlike for smooth fibers, which showed bidirectional transport (Fig. 3a and Supplementary Video 3). To capture the unidirectional transport characteristic resulting from the hemline-shaped fibers, we recorded the flow process using a high-speed camera. Initially, the water droplet coincided with the outline of the rear and was pinned to the top of the hemline sharp edge, as shown in Fig. 3b and Supplementary Video 4a. It then quickly filled the microcavity and spread in the interstice between the fiber and substrate. Because water is pinned at the sharp bottom edge, it can only move in the forward direction. When reaching the sharp bottom edge of the next hemline, the water filled the next microcavity via capillary effects. With continuous water feeding, the water stream advances by flowing into the interstice and consecutively fills the microcavities, thereby achieving continuous liquid transport (Fig. 3c, Supplementary Fig. 9 and Supplementary Video 4b).

Having shown the pinning and advancing dynamics of water on a single fiber attached to a hydrophilic substrate, we next analyzed the impact of fiber geometry on the liquid transport. The driving force for unidirectional liquid spreading is closely associated with the specific geometries of the sharp edges, microcavities and interstices between the fiber and substrate. As illustrated in Fig. 3d, the curvature variation of the menisci at the sharp edge and interstice result in a difference in the Laplace pressure exerted on the liquid, suggesting that the

https://doi.org/10.1038/s44286-023-00001-5

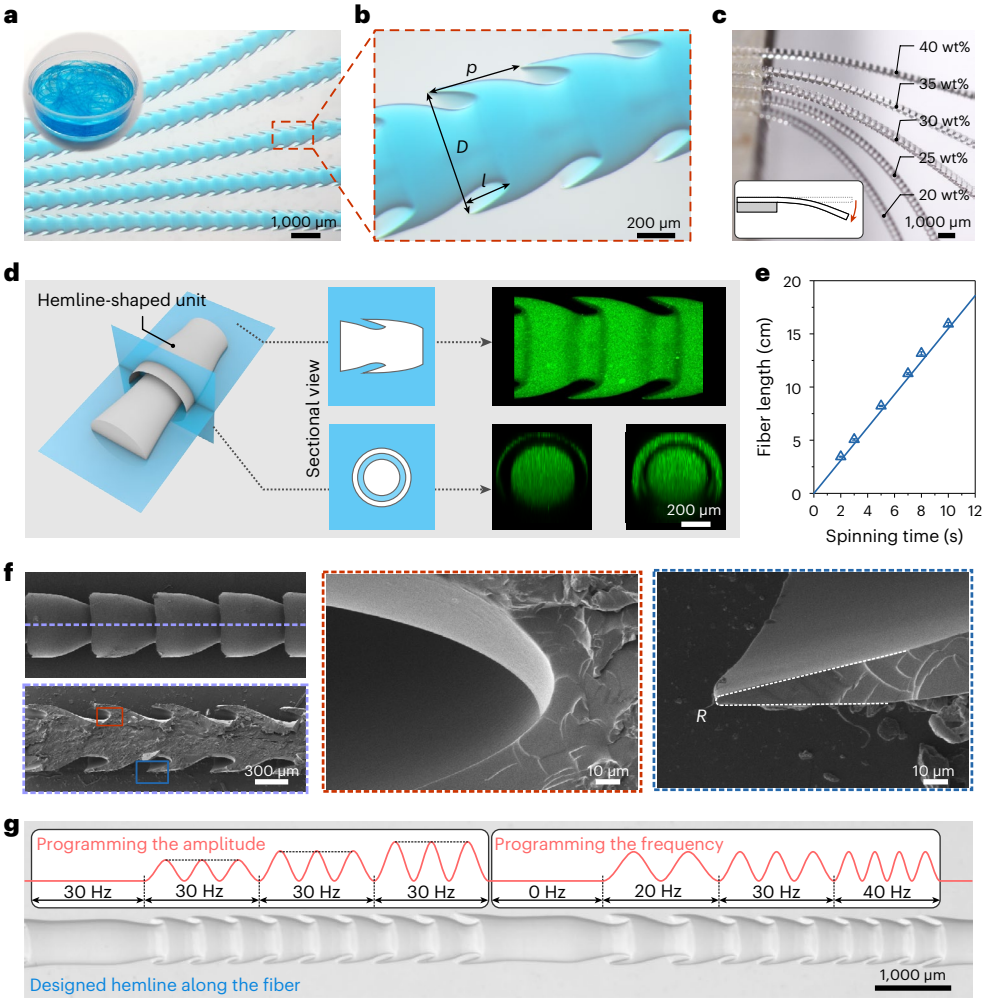

Fig. 2 | Characterization of the hemline-shaped microfibers. a, A batch of microfibers collected from the continuous spinning piezoelectric microfluidic platform. **b**, An optical photograph showcasing resultant microfibers maintaining the hemline microstructure, in which D, l and p represent the fiber diameter, hemline length and pitch, respectively. **c**, Fibers with different PEGDA concentrations showing different flexibility, in which wt% refers percentage by weight. The insert shows the deformation manner of the flexible fiber. With one end stabilized, the fiber can bend itself under the influence of gravity. **d**, Schematic diagram and laser scanning confocal microscope images showing the component homogeneity of the microfiber and the structure detail of the microcavity. **e**, Relationship between the fiber length and the spinning time (Q_i = 15 ml h^{-1}, Q_o = 28 ml h^{-1}); the slope represents the spinning speed of the microfibers. **f**, Scanning electron microscopy images showing the microstructure of the hemline-shaped microfiber. Cutting along the axis (the dashed line in the upper left panel) can showcase the longitudinal section of the fiber (the bottom left panel). The two magnified images demonstrate the details of the corner (region with a red dashed box) and edge (region with a blue dashed box) of the fiber, with a tip radius, R (Q_i = 30 ml h^{-1}, Q_o = 56 ml h^{-1}, f_p = 30 Hz). **g**, A customized microfiber with hemlines of varying length and pitch obtained by programming the input piezoelectric signal. Data points and error bars indicate mean values ± s.d of five measurements in **e**.

wettability of the substrate has a key effect on the spreading process. To quantify such diode-like transport behavior, we deposited a 2.5 µl droplet on the fiber and defined a rectification coefficient, $k = L_f/L_p$, where L_f and L_p represent the transport length of the forward and pinning directions, respectively (Fig. 3e). The unidirectional transport capacity (represented by k) and average liquid transport speed ($\bar{v} = L_f/t$, where t is the spreading time) could be effectively controlled by tuning p and l of the hemline (Fig. 3f,g and Supplementary Discussion II); and p and l were controlled by varying f_p and U, respectively (Supplementary Fig. 10). A smaller p value indicates a decreased distance between two adjacent hemline edges, which may negate the pinning effect and reduce k (Supplementary Fig. 20c). A larger p results in an increased microcavity size, causing a larger amount of liquid to fill the microcavities (Supplementary Fig. 21d,e), thereby decreasing $\bar{v}$. Similarly, a large cavity length, l, tends to make it easier for the leaked liquid to contact the previous hemline. However, a small l and less sharp edge weakens the pinning effect at the contact points, leading to a smaller k. Simultaneously, a larger l would cause a larger amount of liquid to fill the microcavities, thereby decreasing $\bar{v}$.

Because the long-distance transport ability is a key criterion for evaluating practical application of the system, we used a hemline-shaped microfiber with specific morphological features (p and l) to investigate the long-distance transport ability by continuously injecting water from one side. When water was injected into the fiber at a fixed injection flow rate, the water moved in the forward direction (Fig. 3h). Figure 3i and Supplementary Fig. 11 show the transport distance as a function of time for different injection flow rates. Initially, the transport speed is high but decreases in time until a steady-state value is reached. Thus, we next estimated the transport speed under the steady-state condition, expressed as the slope of the curve in the nearly linear region. The transport speed increases with increasing injection flow rate. However, for a specific fiber morphology (p = 418 µm, l = 185 µm) and substrate wettability (θ = 40°), the maximum transport speed was about 5 mm s^{-1}, corresponding to a critical injection flow rate of

https://doi.org/10.1038/s44286-023-00001-5

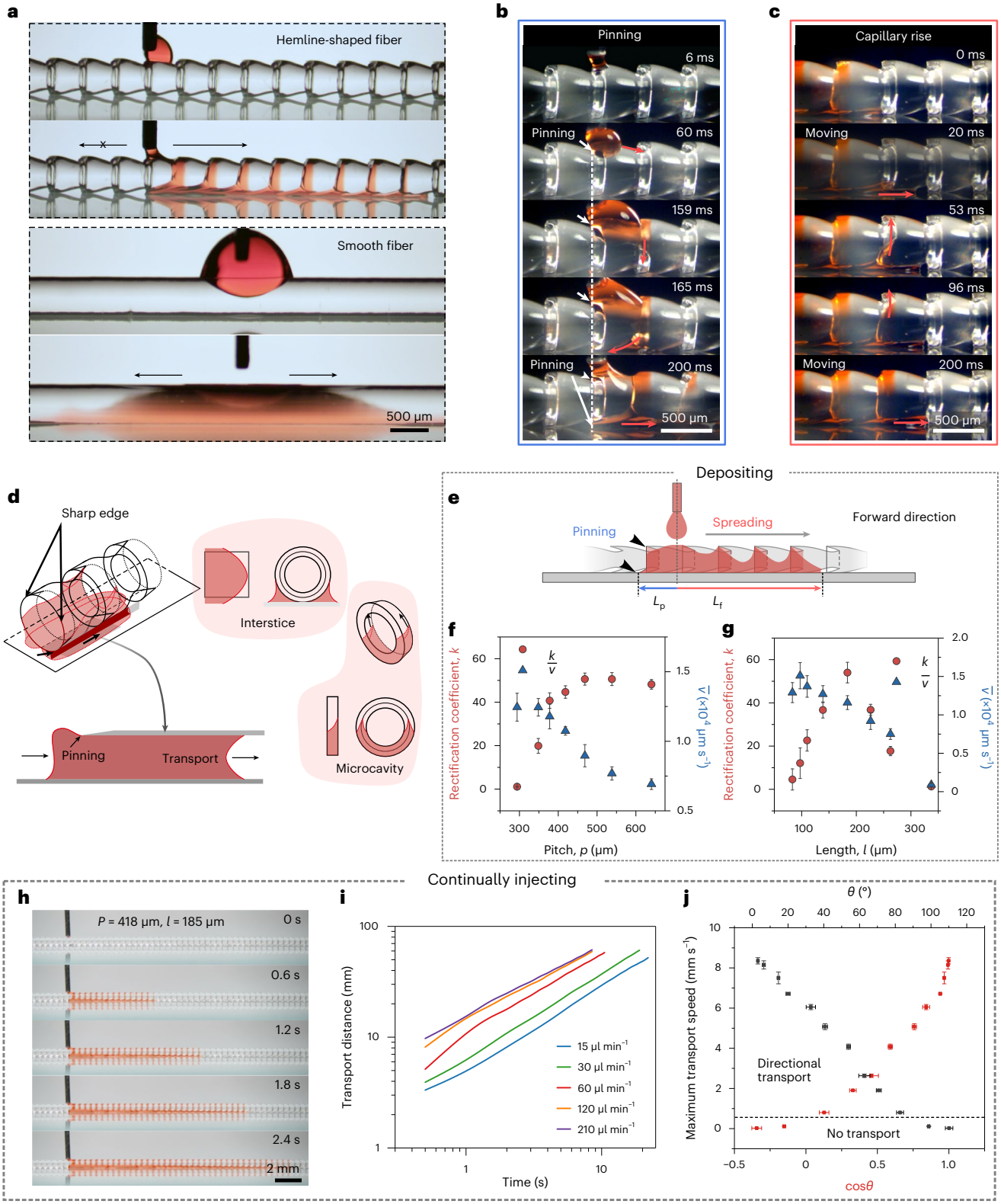

Fig. 3 | Directional liquid transport along a hemline-shaped microfiber attached to a hydrophilic substrate. a, Unidirectional liquid transport behavior along a hemline-shaped fiber and bidirectional transport behavior along a smooth fiber at a hydrophilic substrate. **b**, Time-lapse images showing the pinning effects at the top and bottom sharp edges of the hemline. **c**, Time-lapse images showing the continuous transport behavior along the fiber attached to a glass slide. **d**, Mechanisms responsible for the directional liquid transport, including pinning at the sharp edge, capillary rise that results in the filling of the microcavity, and continuous transport along the interstice between the fiber and substrate. **e**, Illustration of the directional liquid transport when depositing a 2.5 μl droplet on the fiber. **f**,**g**, Plots of rectification coefficient and average transport speed versus the pitch (**f**) and the hemline length of the microfiber (**g**). **h**–**j**, Transport behaviors under continuous injection with the optimized morphology (p = 418 μm, l = 185 μm and the injection flow rate was 30 μl min^{-1}). **h**, Typical time-lapse images of the long-distance unidirectional liquid transport under continuous injection. **i**, A log–log plot of the transport distance as a function of time under different injection flow rates. **j**, Plot of maximum transport speed as a function of θ and cosθ, where θ is the WCA. Data points and error bars indicate mean values ± s.d. of five measurements in **f** and **g**, and three measurements in **j**.

https://doi.org/10.1038/s44286-023-00001-5

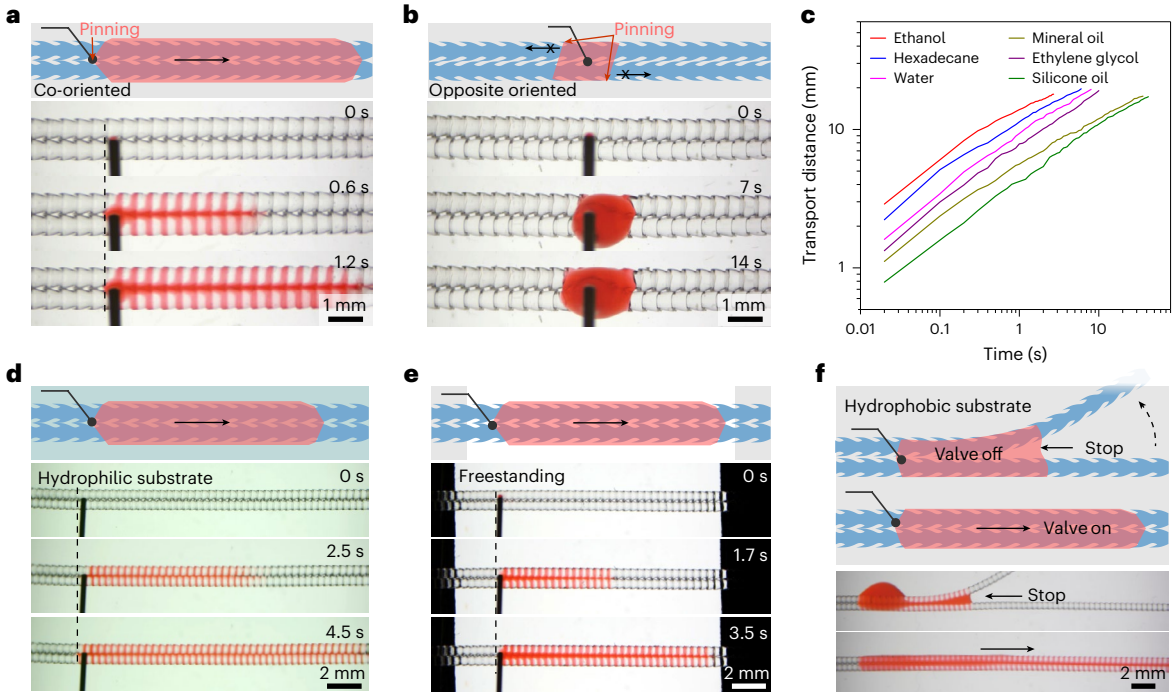

Fig. 4 | Continuous liquid transport on two contacting microfibers. a,**b**, Water transport along contacting co-oriented (**a**) and opposite-oriented (**b**) fibers placed on a hydrophobic substrate. **c**, A log–log plot of transport distance of different liquids as a function of time by depositing 2.5 µl liquid droplets. **d**,**e**, Water transport along two contacting co-oriented fibers placed on a hydrophilic substrate (**d**) and without any substrate (**e**). **f**, On/off control of the transport by dividing apart and bringing together two co-oriented fibers placed on a hydrophobic substrate.

120 µl min^{-1}. Once the injection flow rate exceeded 120 µl min^{-1}, the liquid would overflow to the surroundings (Supplementary Fig. 12), while the forward transport speed was still 5 mm s^{-1}, insensitive to larger injection flow rates. Different maximum transport speeds can be obtained using fibers of differing geometries (Supplementary Fig. 13). Moreover, for fibers with given geometrical parameters, the maximum transport speed could be further adjusted by adjusting the substrate wettability (Supplementary Fig. 14). A more hydrophilic substrate showed a higher maximum transport speed, whereas a substrate having a WCA larger than 90° impeded transport (Fig. 3j).

These results indicate that a single microfiber can achieve unidirectional liquid transport on a hydrophilic substrate (Supplementary Fig. 15). Next, we speculated that a pair of hemline-shaped microfibers can realize directional liquid transport on any substrate because they form an interstice where they are in contact[54]. To validate this, two co-oriented fibers arranged side by side were placed on a hydrophobic substrate. The water deposited on the fibers was unidirectionally transported in the forward direction (Fig. 4a). This can be attributed to the continuous filling of the microcavities and interstices between the two fibers. In contrast, the two oppositely oriented fibers prevented water from spreading in any direction owing to the sharp edge pinning (Fig. 4b). In addition, the co-oriented pair of fibers showed excellent unidirectional liquid transport on hydrophilic substrates (Fig. 4d). Intriguingly, two freestanding co-oriented fibers can guide unidirectional water transport, even without any substrate (Fig. 4e). On this basis, a valve could be created to switch the water transport on and off. As shown in Fig. 4f, water transport stopped when the fibers were separated, whereas it resumed when the fibers were brought back together. This suggests that by simply controlling the interstice between the two fibers, the spatiotemporal manipulation of liquid transport can be achieved. Moreover, the unidirectional transport of different types of liquid was demonstrated for freestanding co-oriented fiber pairs. These include lower-surface-tension liquids, such as ethanol and hexane; higher-viscosity liquids, such as ethylene glycol; and lubricant oils, such as mineral oil and silicone oil (Supplementary Fig. 16). These liquids were transported at different speeds in part because of differences in their viscosity and surface tension (Fig. 4c, Supplementary Fig. 16c and Supplementary Table 2). The driving force for directional liquid spreading is generated by the Laplace pressure difference resulting from the sharp edge of the hemline. For lower-viscosity liquids, such as ethanol, hexadecane and water, those with a lower contact angle with the fibers show higher transport speeds[55]. In contrast, more viscous fluids show slower transport speeds (Supplementary Fig. 16d), consistent with what one might expect from a simple Washburn analysis[56,57].

The spontaneous, unidirectional liquid transport ability imparts the hemline-shaped fibers with broad potential applications, particularly in droplet manipulation, adaptable liquid transport and water/oil separation. To demonstrate this, a pair of co-oriented hemline-shaped fibers was fixed on a hydrophobic plate. The plate served as a stamp to pick up a droplet that was then transported to another plate (Fig. 5a,b and Supplementary Video 5a). As such, complex droplet manipulation can be readily achieved using stamps with as-designed fiber patterns. For example, three pairs of co-oriented hemline-shaped fibers forming separate paths were used to translocate multiple droplets simultaneously (Fig. 5c). In addition, the formation of a converging fiber pattern enabled droplet mixing (Fig. 5d) and a divergent pattern enabled droplet splitting (Fig. 5e). This versatile droplet manipulation is highly appealing for microreactors and open microfluidic applications. Moreover, benefiting from the flexibility of the microfibers, long-distance liquid transport on curved surfaces can be achieved using a pair of contacting co-oriented microfibers, regardless of the surface wettability. Therefore, liquid transport along practical materials was realized (Fig. 5f and Supplementary Video 5b), and the transport path could be customized, enabling spiral, upward and dangling paths (Fig. 5g,h and Supplementary Video 5b,c).

Another distinguishing feature of the hemline-shaped microfibers is their ability to extract water from oil. We found that water passed through the oil deposited on a pair of contacting co-oriented fibers and continued to move, suggesting that water preferentially wetted

https://doi.org/10.1038/s44286-023-00001-5

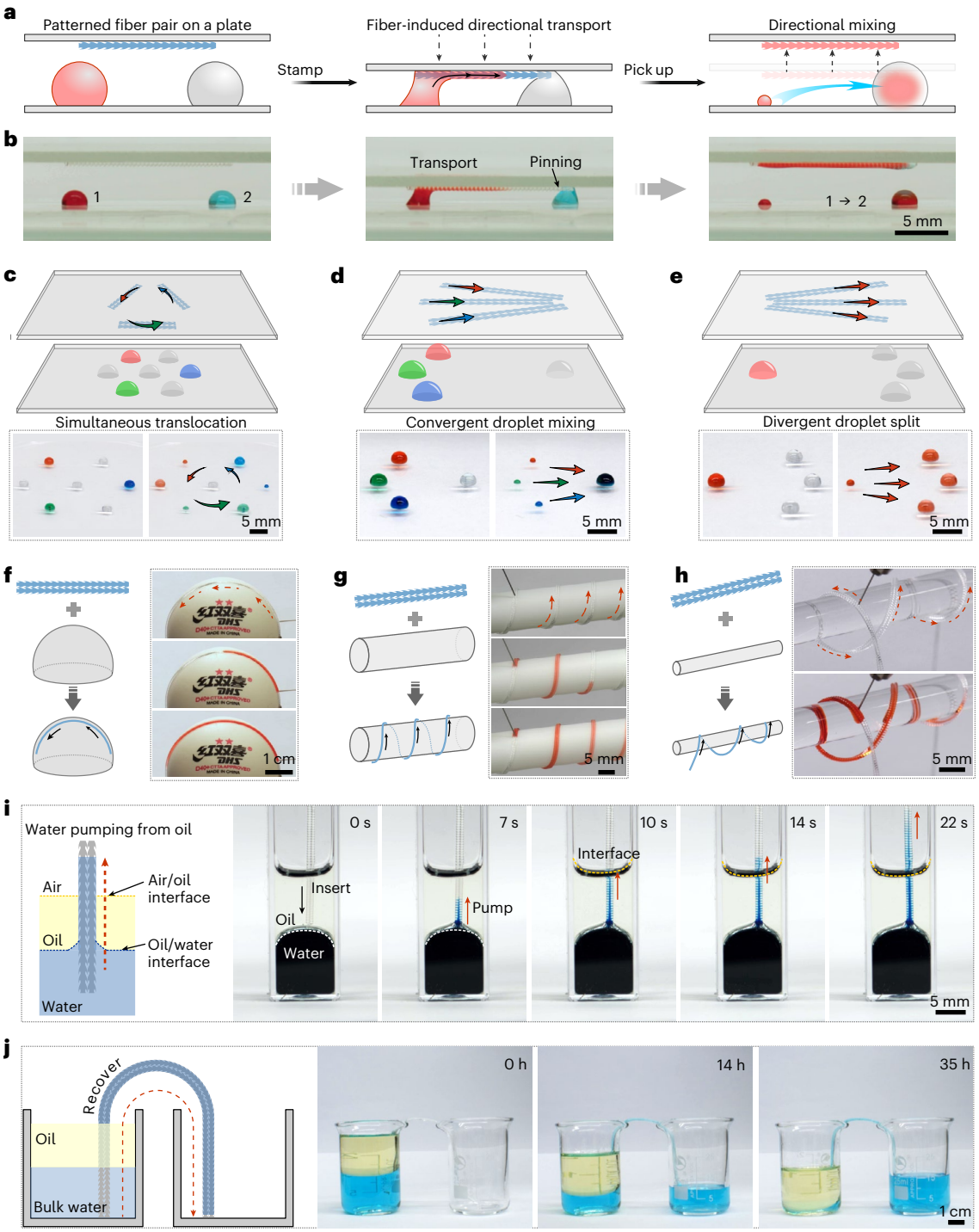

Fig. 5 | Applications of the hemline-shaped fibers bearing unidirectional liquid transport capabilities. a,**b**, Schematics (**a**) and photographs (**b**) showing the fiber-based 'stamps' for droplet manipulation. **c**–**e**, Complex droplet manipulation using stamps with programmable fiber patterns, including simultaneous translocation of multiple droplets (**c**), convergent droplet mixing (**d**) and divergent droplet split (**e**). **f**, Side views of a pair of co-oriented fibers freely attached on a ping-pong ball surface. By continuously depositing dyed water onto one side, water flowed upward and climbed along the curve without retraction at the injection position. **g**,**h**, Water transport on the surface of a straw (**g**) and a glass rod along a spiral or dangling path (**h**). **i**, Water extraction from oil with the aid of a pair of co-oriented fibers. **j**, Bulk water transfer from a thick oil layer by a bundle of co-oriented hemline-shaped fibers.

the fiber surface. In contrast, the predeposited oil was repelled by the advancing water phase (Supplementary Fig. 17). We further confirmed that a pair of contacting co-oriented freestanding fibers enabled unidirectional water transport even when fully submerged in the oil phase (Supplementary Fig. 18). Thus, water can continuously travel along the paired fibers upward across the oil/water interface, as shown in Fig. 5i and Supplementary Video 5i. This provides a solution for water extraction from complex multiphase fluid environments[3]. By applying this, a facile system for bulk water transfer was developed. As shown in Fig. 5j, using a bundle of co-oriented hemline-shaped fibers, water was extracted from a thick oil layer of 2.3 cm, reaching a rising height of about 3.1 cm. Collectively, these features of the hemline-shaped fibers give them broad potential applications in the energy and environmental engineering fields.

Discussion

We have reported a flexible hemline-shaped microfiber prepared using microfluidics for directional liquid transport. The microfibers were generated by combining the piezoelectric-induced vibration of a jet in a microfluidic channel with rapid photopolymerization, resulting in annularly connected microcavities with sharp edges and wedge corners. The unique structural features of the microfibers enable directional water transport because of unilateral pinning. In addition, the structural features of the microfibers were precisely tailored by the microfluidic and piezoelectric parameters, enabling control of the transport capacity and speed. Moreover, the assembly of the fibers facilitated versatile transport regardless of the type of liquid or wettability of the substrate; the flexibility of the fibers enabled substrate-free and underwater transport. Owing to these capabilities, we demonstrated the use of the hemline-shaped microfibers in smart droplet manipulation, versatile liquid transport and water/oil separation.

In general, continuous liquid transport along a surface is driven by designed anisotropic structures[24,58]. Despite the rapid progress in the development of novel liquid transport strategies, many rely on predesigned surfaces with intricate structural features[23,28]. However, the predesigned substrate substantially restricts the transport path and cannot achieve versatile transport on the surface of any object without redesign. In addition, the complex equipment, need for an ultraclean environment and high cost of traditional microfabrication technologies used to generate sophisticated structures restrict their practical usage. Another important point is that each hemline-shaped microfiber is fabricated using microfluidics. Microfluidics has been widely explored for the dynamic manipulation of liquid/liquid interfaces using aqueous two-phase systems under external control. However, this typically requires the strict selection of the liquids used (most commonly poly(ethylene glycol) and dextran)[49,50]. In our study, PEGDA and water were used as the two liquids, making it possible to solidify the liquid jet directly to obtain the fibers.

Taken together, the directional liquid transport performance of hemline-shaped fibers, along with their ease of fabrication, universality and scalability, will enable widespread applications, including open microfluidics, water extraction and real-life liquid transport, especially in substrate- or surface-limited settings. Future work could focus on coupling this method with other techniques, such as 3D printing, by which fiber networks could be directly printed for water transport along predetermined paths. To extend the potential applications of this technology, stimuli-responsive functional materials could be incorporated into the inner phase to develop smart hemline-shaped microfibers. We anticipate that other types of UV-curable liquid can be used to fabricate fibers with distinct properties using our microfluidic platform.

Methods

Materials

PEGDA (number-average molecular weight, M_n = 700) and HMPP were purchased from Sigma-Aldrich. Citrate sodium, hexane, ethanol, ethylene glycol and mineral oil were purchased from Macklin. Silicone oil (50 cS) was obtained from Shin-Etsu Chemical. Fluorescent polystyrene nanoparticles (F8811) were purchased from Invitrogen for the laser scanning confocal microscopy image. Polydimethylsiloxane (PDMS; Sylgard 184) was obtained from Dow Corning. Ultrapure water (resistivity 18.2 MΩ cm) was obtained using a Millipore Milli-Q system.

Piezoelectric microfluidic system

To observe the jet, capillary microfluidics were achieved by coaxially assembling two capillaries on a glass slide. Briefly, a cylindrical capillary (inner diameter 580 µm, outer diameter 1.0 mm; World Precision Instruments) was tapered and polished to a tip with a 50 µm inner diameter using a capillary puller (Sutter Instrument, P-97) and a microforge (Narishige, MF-830); this was used as the injection tube. The other cylindrical capillary, which had inner and outer diameters of 800 µm and 1.0 mm, respectively, served as the collection tube. The two capillaries were aligned inside a square capillary (AIT Glass) with an inner diameter of 1.05 mm.

For fabricating hemline-shaped microfibers, the tip of the injection tube was 200 µm and the inner diameter of the collection tube was 1,560 µm; no square capillary was used. These dimensions allow the preparation of fibers with a large range of diameters. The microfluidic chip was placed vertically and immersed in 2 wt% sodium citrate solution to counteract the force of gravity of the PEGDA fibers. Transparent epoxy resin was used to seal the joints of the capillaries where necessary.

A piezoelectric stack (Core Morrow Technology, PSt150/7/20VS12) was used to transmit the programmable signal and modulate the inner fluid through contact with a thin polytetrafluoroethylene film (thickness of about 100 µm). The film periodically squeezed the fluid and coupled the piezoelectric vibrations into the flow, as shown in Supplementary Fig. 1. The stack was controlled by a signal generator (Siglent, SDG 2000X) using a power amplifier (Core Morrow, E-05). The amplification factor of the power amplifier was constant at 12.

UV irradiation set-up

The set-up consisted of two UV light heads (365 nm, EXFO OmniCure SERIES 1000) mounted on homemade holders surrounding the collection tube in opposite directions (Supplementary Fig. 3). UV light was blocked from the tip of the inner capillary using heavy-duty black electrical tape (3M) to prevent clogging.

Characterization of the hemline-shaped jet/microfiber

The flow behavior of the hemline-shaped jet was monitored using an inverted microscope equipped with a high-speed camera (AcutEye). The fluorescence images of the hemline-shaped microfibers were obtained using a laser scanning confocal microscope (Nikon, A1). The microstructures of the solidified microfibers were observed by scanning electron microscopy (HITACHI, SU8010).

Tracking the liquid transport dynamics

The resultant hemline-shaped fibers were washed ten times to remove sodium citrate from the surfaces. Before performing a liquid unidirectional transport experiment, Kimwipes were used to absorb any surface water. In addition, we captured the transport and pinning behavior of water with red food dye (0.05 mg ml^{-1}) at room temperature. For droplet depositing, a water droplet (2.5 µl) was suspended at the tip of the needle, and then placed directly in contacted with the fiber. Regarding the calculation of k, we recorded the corresponding value of L_p and L_f. For continuous injection, water was pumped through a stainless-steel needle at a variable flow rate (ranging from 30 µl min^{-1} to 210 µl min^{-1}) using a syringe pump (LSP01-2A, Longer). To observe the water pinning effect at the sharp edge and the transport dynamics of the hemline, we continuously injected water on the fiber and monitored the moving boundary of the water using the high-speed camera (FASTCAM SA4, Photron).

Wettability measurements

A gradient wetting substrate was formed by mixing and degassing a PDMS precursor (part A) and curing agent (part B) in a mass ratio of 10:1. A wettability gradient was achieved using radiofrequency plasma (DT-01, Ops) at a power of 2 W for treatment times ranging from 0 to 40 s. Subsequently, the PDMS plates were immediately used to conduct the water transport experiments, and their contact angles were measured by placing a droplet (1 µl) on the surface and using an optical angle-measuring system (JGW-360D, Kaosi).

Fiber-based 'stamps' for droplet manipulation

Several water droplets (6 µl) were predeposited on a hydrophobic PDMS substrate at a distance of 15 mm. Then the co-oriented fiber

pairs, arranged in a predesigned pattern, were attached to the bottom of the upper plate (a glass slide) by double-sided tape, thus forming the fiber-based 'stamps'. The operation of the 'stamp' involved the use of a displacement platform, which aligned the fibers and the droplets in the vertical direction, and then descended the upper plate to contact the droplet and, finally, lifted it up after the transport process was completed.

Water extraction from oil

For observation, a pair of co-oriented fibers was inserted vertically and submerged below the oil/water interface. For bulk water transfer, the tail end of a bundle of co-oriented fibers (nine fibers) was inserted at the bottom of a beaker containing the water and oil phases, and the other end was placed at the bottom of an empty beaker. Before performing the experiments, the fibers were gently wiped with Kimwipes to remove surface water.

Data availability

All data are available within the paper and its Supplementary Information.

References

1. Feng, S. et al. Three-dimensional capillary ratchet-induced liquid directional steering. *Science* **373**, 1344–1348 (2021).
2. Li, S. et al. Hydrophobic polyamide nanofilms provide rapid transport for crude oil separation. *Science* **377**, 1555–1561 (2022).
3. Fu, C., Gu, L., Zeng, Z. & Xue, Q. Simply adjusting the unidirectional liquid transport of scalable janus membranes toward moisture-wicking fabric, rapid demulsification, and fast oil/water separation. *ACS Appl. Mater. Interfaces* **12**, 51102–51113 (2020).
4. Cacucciolo, V. et al. Stretchable pumps for soft machines. *Nature* **572**, 516–519 (2019).
5. Dudukovic, N. A. et al. Cellular fluidics. *Nature* **595**, 58–65 (2021).
6. Raux, P. S., Gravelle, S. & Dumais, J. Design of a unidirectional water valve in *Tillandsia*. *Nat. Commun.* **11**, 396 (2020).
7. Chen, H. et al. Continuous directional water transport on the peristome surface of *Nepenthes alata*. *Nature* **532**, 85–89 (2016).
8. Van Erp, R., Soleimanzadeh, R., Nela, L., Kampitsis, G. & Matioli, E. Co-designing electronics with microfluidics for more sustainable cooling. *Nature* **585**, 211–216 (2020).
9. Yafia, M. et al. Microfluidic chain reaction of structurally programmed capillary flow events. *Nature* **605**, 464–469 (2022).
10. Aleman, J., Kilic, T., Mille, L. S., Shin, S. R. & Zhang, Y. S. Microfluidic integration of regeneratable electrochemical affinity-based biosensors for continual monitoring of organ-on-a-chip devices. *Nat. Protoc.* **16**, 2564–2593 (2021).
11. Battat, S., Weitz, D. A. & Whitesides, G. M. An outlook on microfluidics: the promise and the challenge. *Lab Chip* **22**, 530–536 (2022).
12. Hou, X. et al. Dynamic air/liquid pockets for guiding microscale flow. *Nat. Commun.* **9**, 733 (2018).
13. Kong, T., Shum, H. C. & Weitz, D. A. The fourth decade of microfluidics. *Small* **16**, 2000070 (2020).
14. Cira, N. J., Benusiglio, A. & Prakash, M. Vapour-mediated sensing and motility in two-component droplets. *Nature* **519**, 446–450 (2015).
15. Malinowski, R., Parkin, I. P. & Volpe, G. Nonmonotonic contactless manipulation of binary droplets via sensing of localized vapor sources on pristine substrates. *Sci. Adv.* **6**, eaba3636 (2020).
16. Lagubeau, G., Le Merrer, M., Clanet, C. & Quéré, D. Leidenfrost on a ratchet. *Nat. Phys.* **7**, 395–398 (2011).
17. Ichimura, K., Oh, S.-K. & Nakagawa, M. Light-driven motion of liquids on a photoresponsive surface. *Science* **288**, 1624–1626 (2000).
18. Xu, W. et al. Triboelectric wetting for continuous droplet transport. *Sci. Adv.* **8**, eade2085 (2022).
19. Li, W., Tang, X. & Wang, L. Photopyroelectric microfluidics. *Sci. Adv.* **6**, eabc1693 (2020).
20. Kwon, G. et al. Visible light guided manipulation of liquid wettability on photoresponsive surfaces. *Nat. Commun.* **8**, 14968 (2017).
21. Lv, J. A. et al. Photocontrol of fluid slugs in liquid crystal polymer microactuators. *Nature* **537**, 179–184 (2016).
22. Parker, A. R. & Lawrence, C. R. Water capture by a desert beetle. *Nature* **414**, 33–34 (2001).
23. Dai, H., Dong, Z. & Jiang, L. Directional liquid dynamics of interfaces with superwettability. *Sci. Adv.* **6**, eabb5528 (2020).
24. Chu, K.-H., Xiao, R. & Wang, E. N. Uni-directional liquid spreading on asymmetric nanostructured surfaces. *Nat. Mater.* **9**, 413–417 (2010).
25. Ju, J. et al. A multi-structural and multi-functional integrated fog collection system in cactus. *Nat. Commun.* **3**, 1247 (2012).
26. Li, J. et al. Topological liquid diode. *Sci. Adv.* **3**, eaao3530 (2017).
27. De Jong, E., Wang, Y., Den Toonder, J. M. J. & Onck, P. R. Climbing droplets driven by mechanowetting on transverse waves. *Sci. Adv.* **5**, eaaw0914 (2019).
28. Liu, M., Wang, S. & Jiang, L. Nature-inspired superwettability systems. *Nat. Rev. Mater.* **2**, 17036 (2017).
29. Shi, Z., Tang, Z., Xu, B., Jiang, L. & Liu, H. Bioinspired directional liquid transport induced by the corner effect. *Nano Res.* **16**, 3913–3923 (2023).
30. Luan, K. et al. Spontaneous directional self-cleaning on the feathers of the aquatic bird *Anser cygnoides domesticus* induced by a transient superhydrophilicity. *Adv. Funct. Mater.* **31**, 2010634 (2021).
31. Tang, Z. et al. Bioinspired robust water repellency in high humidity by micro-meter-scaled conical fibers: toward a long-time underwater aerobic reaction. *J. Am. Chem. Soc.* **144**, 10950–10957 (2022).
32. Meng, Q. et al. Controlling directional liquid transport on dual cylindrical fibers with oriented open-wedges. *Adv. Mater. Interfaces* **9**, 2101749 (2022).
33. Zheng, Y. et al. Directional water collection on wetted spider silk. *Nature* **463**, 640–643 (2010).
34. Nunes, J. K. et al. Fabricating shaped microfibers with inertial microfluidics. *Adv. Mater.* **26**, 3712–3717 (2014).
35. Shang, L. et al. Spinning and applications of bioinspired fiber systems. *ACS Nano* **13**, 2749–2772 (2019).
36. Tian, Y. et al. Large-scale water collection of bioinspired cavity-microfibers. *Nat. Commun.* **8**, 1080 (2017).
37. Li, J., Li, J., Sun, J., Feng, S. & Wang, Z. Biological and engineered topological droplet rectifiers. *Adv. Mater.* **31**, 1806501 (2019).
38. Liu, M. et al. Inhibiting random droplet motion on hot surfaces by engineering symmetry-breaking Janus-mushroom structure. *Adv. Mater.* **32**, 1907999 (2020).
39. Zhang, C. et al. Bioinspired anisotropic slippery cilia for stiffness-controllable bubble transport. *ACS Nano* **16**, 9348–9358 (2022).
40. Wu, S. et al. Superhydrophobic photothermal icephobic surfaces based on candle soot. *Proc. Natl Acad. Sci. USA* **117**, 11240–11246 (2020).
41. Oh, I. et al. Dynamically actuated liquid-infused poroelastic film with precise control over droplet dynamics. *Adv. Funct. Mater.* **28**, 1802632 (2018).
42. Xu, B. et al. Electrochemical on-site switching of the directional liquid transport on a conical fiber. *Adv. Mater.* **34**, 2200759 (2022).
43. Li, C. et al. Bioinspired inner microstructured tube controlled capillary rise. *Proc. Natl Acad. Sci. USA* **116**, 12704–12709 (2019).
44. Li, J. et al. Nature-inspired reentrant surfaces. *Prog. Mater Sci.* **133**, 101064 (2023).

45. Yu, Y. et al. Simple spinning of heterogeneous hollow microfibers on chip. *Adv. Mater.* **28**, 6649–6655 (2016).
46. Du, X. Y., Li, Q., Wu, G. & Chen, S. Multifunctional micro/nanoscale fibers based on microfluidic spinning technology. *Adv. Mater.* **31**, 1903733 (2019).
47. Paulsen, K. S., Di Carlo, D. & Chung, A. J. Optofluidic fabrication for 3D-shaped particles. *Nat. Commun.* **6**, 6976 (2015).
48. Amini, H. et al. Engineering fluid flow using sequenced microstructures. *Nat. Commun.* **4**, 1826 (2013).
49. Chao, Y. & Shum, H. C. Emerging aqueous two-phase systems: from fundamentals of interfaces to biomedical applications. *Chem. Soc. Rev.* **49**, 114–142 (2020).
50. Mak, S. Y., Li, Z., Frere, A., Chan, T. C. & Shum, H. C. Musical interfaces: visualization and reconstruction of music with a microfluidic two-phase flow. *Sci. Rep.* **4**, 6675 (2014).
51. Sauret, A. & Shum, H. C. Beating the jetting regime. *Int. J. Nonlinear Sci. Numer. Simul.* **13**, 351–362 (2012).
52. Weislogel, M. M. & Lichter, S. Capillary flow in an interior corner. *J. Fluid Mech.* **373**, 349–378 (1998).
53. Weislogel, M. M. Compound capillary rise. *J. Fluid Mech.* **709**, 622–647 (2012).
54. Wang, K., Sanaei, P., Zhang, J. & Ristroph, L. Open capillary siphons. *J. Fluid Mech.* **932**, R1 (2022).
55. Liu, Y. et al. Bionic jaw-like micro one-way valve for rapid and long-distance water droplet unidirectional spreading. *Nano Lett.* **23**, 5696–5704 (2023).
56. Washburn, E. W. The dynamics of capillary flow. *Phy. Rev.* **17**, 273–283 (1921).
57. Courbin, L., Bird, J. C., Reyssat, M. & Stone, H. A. Dynamics of wetting: from inertial spreading to viscous imbibition. *J. Phys. Condens. Matter* **21**, 464127 (2009).
58. Zhang, L. et al. Bioinspired unidirectional liquid transport micro-nano structures: a review. *J. Bionic Eng.* **18**, 1–29 (2021).

Acknowledgements

This work was supported by the National Natural Science Foundation of China with grants T2225003 (Y.Z.), 22202050 (C.Y.), 32271383 (L.S.) and 52073060 (Y.Z.), and the National Key Research and Development Program of China with grant 2020YFA0908200 (Y.Z.).

Author contributions

Y.Z. and L.S. conceived the idea. C.Y. designed the experiments. C.Y. and Y.Y. conducted the experiments. C.Y. and L.S. analyzed the data. C.Y., L.S. and Y.Z. wrote the paper.

Competing interests

The authors declare no competing interests.

Additional information

Supplementary information The online version contains supplementary material available at https://doi.org/10.1038/s44286-023-00001-5.

Correspondence and requests for materials should be addressed to Luoran Shang or Yuanjin Zhao.

Peer review information *Nature Chemical Engineering* thanks Huan Liu and the other, anonymous, reviewer(s) for their contribution to the peer review of this work.